CHAPTER 7. Electrochemical functionality of spiropyran SAMs on gold

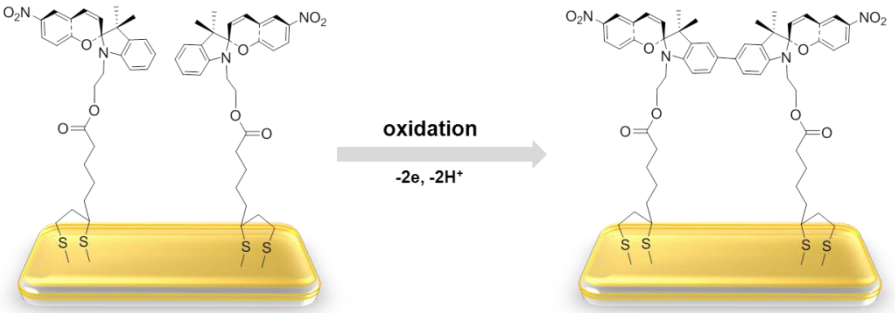

Photochromism in self-assembled monolayers of spiropyran has attracted substantial attention in recent years, however the electrochemistry of the spiro- compounds has not received much consideration to date. In this chapter we explore the electrochemical oxidation of self-assembled monolayers of 6-nitro BIPS spiropyran (SP) prepared on polycrystalline gold surfaces. SAMs were characterized with cyclic voltammetry, X-ray photoelectron spectroscopy (XPS), surface enhanced Raman scattering (SERS) and UV/vis absorption spectroelectrochemistry. Electrochemical oxidation of spiropyrans in solution results in aryl C-C coupling and the formation of a symmetric spiropyran dimer, as was shown in chapter 6. Comparison of spectroscopic data for spiropyran dimers in solution and in monolayers confirms that similar oxidative coupling occurs in the SAMs on gold also. The dimer formed can be electrochemically oxidized to monocationic and dicationic states and shows remarkable stability under UHV and ambient conditions in all those redox states. In addition, the dimerized spiropyran SAM shows photochromism, which was characterized by XPS and SERS spectroscopy. In conclusion, the photochemical and electrochemical functionality of spiropyran SAMs is demonstrated to show potential for application as dual responsive materials.

The results presented in this chapter are in preparation for publication.

7.1 Introduction

Molecular switches are organic compounds that allow the control of molecular structure and function with external stimuli - light (photochromism), potential (electrochromism), pH (acidochromism), solvent (solvatochromism) and temperature (thermochromism) due to changes in bonding and/or redox state. In some cases more than one stimulus type can bring the molecule into a new state providing a multiresponsiveness to a material.

Dual responsive (photo- and redox-active) materials are attractive because they offer the possibility to combine light, which non-destructively addresses the chromophore, and a potential to access different oxidation states for molecular memory applications. Remarkable examples of such smart materials are azobenzenes, which undergo photochemical trans-cis isomerization and reductively form hydrazobenzene, in a reversible manner [1]. Another, more complex system with four accessible states is the overcrowded alkene *bis*-thiaxanthylidene, where the conformationally unstable *syn*-folded state is generated photochemically, while dicationic and twisted form result from oxidation and reduction [2,3]. Dithienylethenes have been shown to constitute a versatile platform for photo-electrochemical control over materials' properties also [4].

Spiropyrans are well known for their photochromism, which can be utilized in the solid state [5], solution [6], polymers [7,8] and monolayers [9,10]. The reversible photochromism of spiropyrans consists of switching between the ring-closed stable form where the indoline and chromene moieties are orthogonal and the ring-open thermally unstable form with a planar configuration (Scheme 7.1), induced by UV/vis light, respectively [11]. Acidochromism [12], solvatochromism [13] and response to the presence of metal ions [14] have been demonstrated as well. In acidic environments the chromene oxygen of the MC form becomes protonated, which has been used in a SAM- functionalized electrode [15]. A monolayer on an electrode surface converted to the merocyanine form can be switched between zwitterionic (N^+ and O^-) (Scheme 7.1) and protonated merocyanine forms (N^+ and OH) by variation of the pH of the solution, thus giving a photochemical and pH-controllable electrode [15].

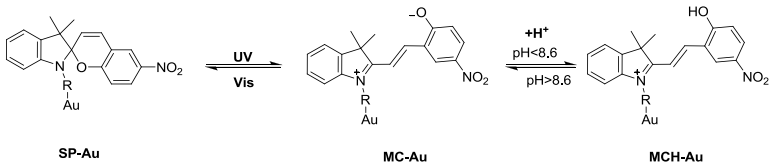

Scheme 7.1 Photochromism and acidochromism of spiropyran.

In contrast, uncertainty in the literature concerning the mechanisms that follow oxidation of spiropyrans in solution has limited the development of this aspect and the utilization of spiropyrans for electrochromic applications. The first reports on multistimuli control of switching of spiropyrans emerged in 1996. Zhi *et al.* suggested the formation of

the radical anion upon reduction of the spiropyran at *ca.* -1 V *vs.* Ag/AgCl, which results in ring-opening to the MC form [16]. A similar hypothesis was proposed for the oxidation to the SP radical cation, which was reported to undergo ring-opening to the MC form and, in the presence of water, irreversible dimerization at the chromene moiety via formation of a C-O-C linkage [17]. The second hypothesis rationalized the irreversible electrochemistry, where oxidation at *ca.* 1 V *vs.* SCE leads to a chemical reaction comprising ring-opening and possible formation of π-radical cation dimers of the MC form [18].

Our own spectroscopic and electrochemical study reported in chapter 6 has shown that oxidation of spiropyran in solution results in formation of a symmetric spiropyran dimer via aryl C-C coupling, but does not lead to ring opening to a merocyanine monomer or dimer, in contrast to earlier hypotheses. In brief, it has been shown that oxidation of spiropyrans in solution proceeds via a sequence of electrochemical (E) and chemical reaction steps (C) resulting in a four step ECCE mechanism. An example is the oxidation of **1** illustrated in Figure 7.1. The initial oxidation of the indoline nitrogen at *ca.* 1 V (electrochemical step) is irreversible due to the subsequent fast chemical reactions, in which the oxidized nitrospiropyran radical cation $\mathbf{1}^{+\cdot}$ dimerizes by aryl C-C coupling (1^{st} chemical step) to form $H_2\mathbf{2}^{2+}$ and spontaneously deprotonates twice to form **2** (2^{nd} chemical step). The dimer (**2**) obtained is symmetrical and exhibits two reversible one-electron oxidation waves at potential lower than for **1**. The first one-electron oxidation of **2** at 0.7 V generates the radical cation ($\mathbf{2}^{+\cdot}$). The second one-electron oxidation at 0.88 V yields a symmetric dication $\mathbf{2}^{++}$ and the two indoline moieties adopt a quinoidal structure.

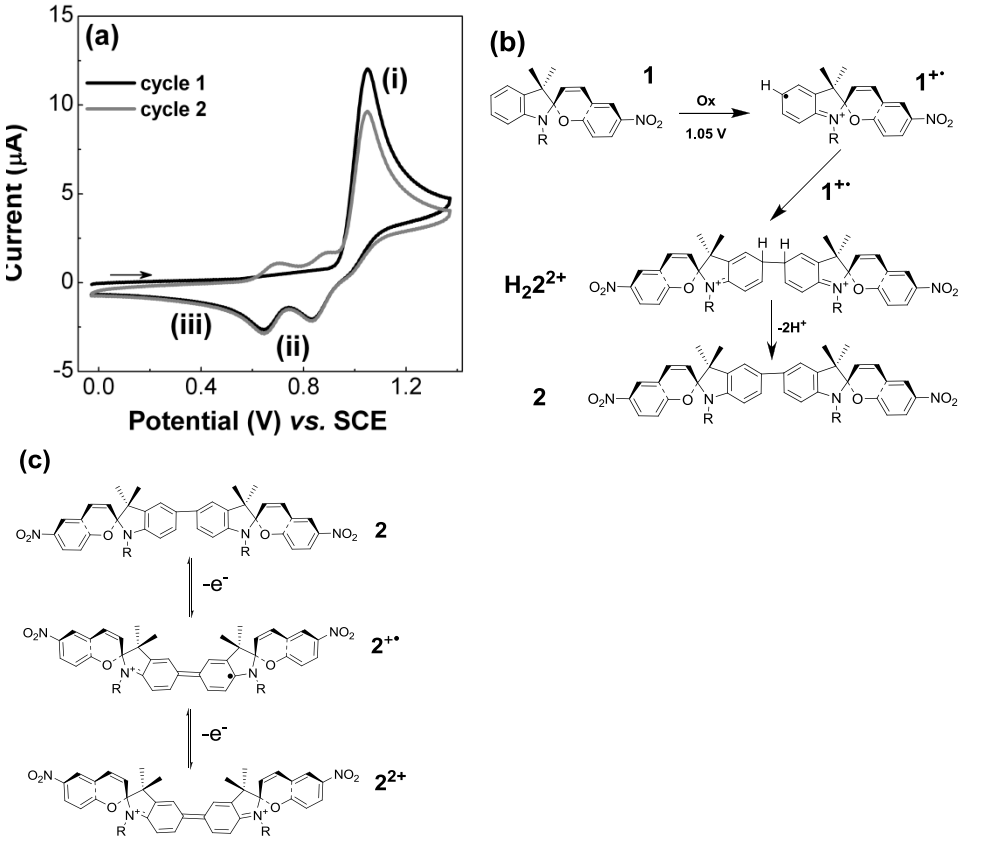

Figure 7.1 Cyclic voltammogram of spiropyran **1** in solution (a). Cyclic voltammetry of **1** at a glassy carbon electrode in 1,2-dichloroethane (0.1 M $TBAPF_6$) (in an O_2 and H_2O free solution). (b) The oxidation observed at 1.0 V in the CV of **1** (Figure 7.1(a)) can be assigned as an overall 4 e^- ECCE process (E: one e^- oxidation of two molecules of **1**, C: dimerization of **1** to form H_2**2**, C: double deprotonation to form **2**, E: two e^- oxidation of **2** to form $\mathbf{2}^{2+}$), see (c). At point (ii) and (iii) in the CV (a), $\mathbf{2}^{2+}$ undergoes one e^- reduction to $\mathbf{2}^{+\cdot}$ and **2**, respectively. (c) Reversible oxidation of obtained dimers **2** to dication with formation of intermediate radical cation $\mathbf{2}^{+\cdot}$.

Monolayers of photoactive and redox-active compounds are often studied to understand the molecular behaviour in a confined microenvironment that resembled environment found in applications but can also serve as model for behaviour of polymeric systems or other environments. Depending on the functional/terminal groups attached to the redox centre, self-assembly can results in inhibition of proton or electron transfer [19], thus completely blocking the redox activity; or tight surface packing can result in hindered molecular motion and increased stability of intermediate high energy conformational states [3].

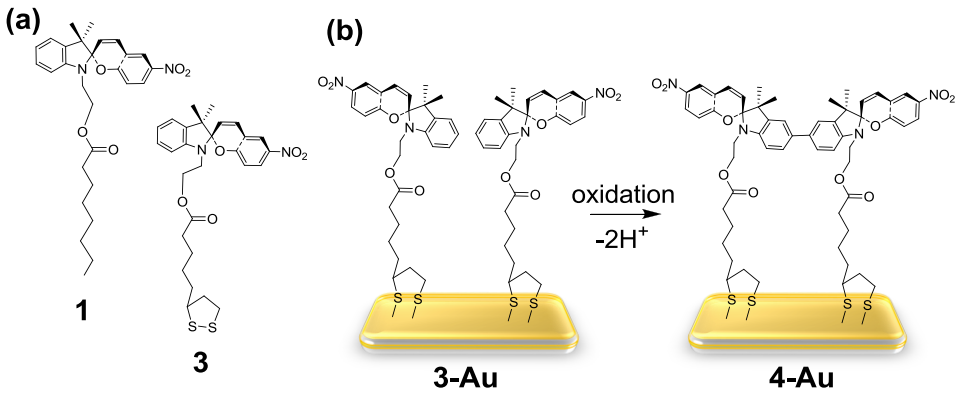

Figure 7.2 (a) Structure of spiropyrans **1** and **3** and (b) electrochemically induced dimerization in a SAM of **3**-Au to form **4**-Au.

Solution studies provided a reference point for what can be expected after the immobilization of the spiropyran on a surface. The dimerization of **1** in solution raises important questions with regards to the utilization of this compound in many surface studies: Can dimerization proceed in self-assembled monolayers, where the mobility of the monomers is hampered by surface attachment and steric interactions? Can it be blocked by tuning the surface density of **1** by mixing with alkane thiols? And finally, considering possible applications, how stable are the (di-)cationic species obtained in the monolayer. To answer these questions we prepared spiropyran **3** [20], which bears a disulfide linker for self-assembly on Au surfaces – Au/mica, semi-transparent Au/glass, and roughened Au bead electrodes (Figure 7.2) and analysed the SAMs formed spectroscopically and electrochemically.

7.2 Results

Cyclic voltammograms of spiropyran SAMs on Au

The cyclic voltammogram (CV) of **3**-Au (Figure 7.3a) is consistent with the cyclic voltammogram obtained for **1** in solution (Figure 7.1) – irreversible oxidation at 1.05 V vs. SCE is followed be a chemical reaction to yield a product with two reversible electrochemical redox processes at E_{pa} 0.8 V and 0.92 V. The irreversibility of the initial oxidation is apparent in the absence of an oxidation wave at 1.05 V on the second cycle even at increased scan rates 1-15 V s^{-1} (Figure 7.3b). A minor (+0.08 V) shift in the E_{pa} related to the spiropyran oxidation at higher scan rates was observed, while product redox waves (below 1 V) remain unaffected, pointing to limited electron transfer at higher SR. Similar effects were observed in solution. As reported in the literature for the indoline analogue *N,N'*-dimethylaniline, which undergoes oxidative C-C coupling to produce the symmetric dimer tetramethylbenzidine, electrochemistry is irreversible up to scan rates of 500 V s^{-1} [21,22,23]. The similarity of the cyclic voltammetry of **1** in solution, where an

ECCE process is observed, and that of **3** in the SAM suggest that a similar oxidative dimerization process occurs in the SAMs (Figure 7.2b). The charge transferred during the oxidation at 1.05 V is twice more than the charge transferred in the two reduction steps, which is consistent with an initial one electron oxidation of two spiropyrans ($-2e^-$), dimerization and deprotonation to yield a neutral dimer and immediate reoxidation of the dimer at the same potential ($-2e^-$) and final two step reduction ($+e^-$ and $+e^-$), thus $-4e^-/+2e^-$. The surface coverage of **3** on Au calculated from the spiropyran oxidation at 1.05 V, considering that each molecule oxidizes twice in this step, is $(6 \pm 1)*10^{-11}$ mol cm^{-2}, and for **4** – $(3 \pm 0.5)*10^{-11}$ mol cm^{-2}. The area occupied by each monomer of **3** is 3.3 nm^2. The absence of the oxidation wave at 1.05 V on the second oxidation cycle gives evidence that no monomeric spiropyran remains in the SAM. The latter observation suggests that a high degree of flexibility and mobility of **3**-Au, which upon oxidation undergoes fast coupling (>140 s^{-1}).

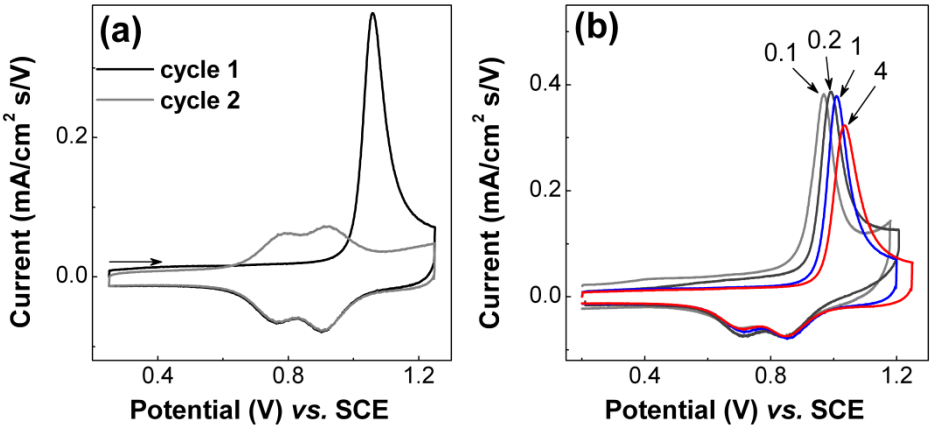

Figure 7.3 Cyclic voltammogram of SAM **3**-Au/mica measured in acetonitrile (0.1 M $TBAPF_6$) at a scan rate of 1.0 V/s (a) and at a scan rate of 0.1, 0.2, 1.0, and 4.0 V/s (b).

SERS spectroelectrochemistry of SAMs on roughened Au bead electrodes

The redox chemistry of a SAM of **3** on a roughened Au bead was studied by surface enhanced Raman scattering (SERS) spectroscopy. Initially the SERS spectrum consists of features of the ring-closed spiropyran with characteristic asymmetric and symmetric nitro bands at 1578 cm^{-1} and 1335 cm^{-1}, and a few other bands typical of SP at 1227 cm^{-1} and 1650 cm^{-1} (Figure 7.4a (i)).

Two cycles of the cyclic voltammetry were performed in dichloromethane (0.1 M $TBAPF_6$) (Figure 7.4b). In the first sweep, a maximum positive potential was set at 1.1 V (1) and in the second it was at 1.3 V (2). The first cycle shows only partial oxidation of the SAM while the second cycle shows complete oxidation of the SAM, as can be seen from the residual spiropyran oxidation wave at 1.05 V, which follows the two oxidation waves at

0.75 and 0.92 V of the dimer. This allowed the progressive formation of the dimer product to be monitored by SERS spectroscopy (Figure 7.4a).

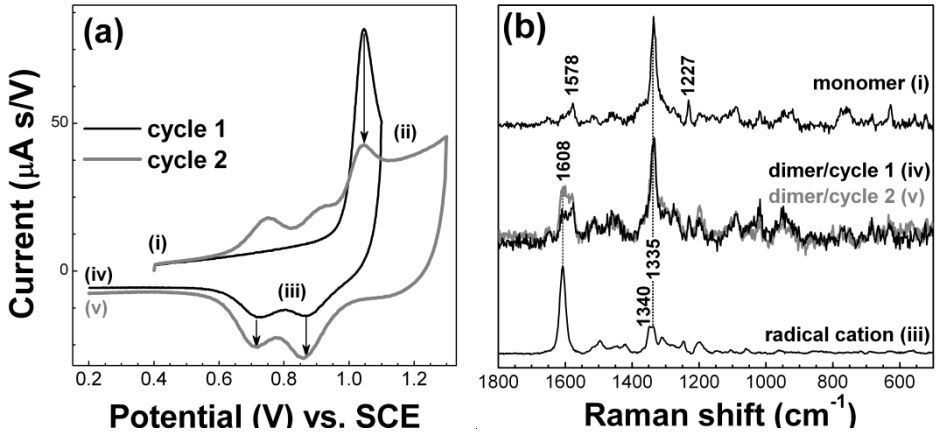

Figure 7.4 (a) Cyclic voltammograms of a SAM of **3** on a roughened Au bead acquired over a narrow (1) and wider potential window (2) measured in dichloromethane (0.1 M $TBAPF_6$). (b) SERS spectra of a SAM of **3** on a roughened Au bead measured initially (i), after conversion to dimer (iv) and (v), and after reduction at 0.8 V (iii) Spectrum (iii) was scaled 1/300 times for comparison.

The SERS spectrum of the SAM after cyclic voltammetry (cycle 1) is presented in Figure 7.4a (iv). After the redox cycle the spectrum of the SAM is similar to that of the initial spectrum, but with one new band at 1608 cm^{-1}.

A second cycle to a higher overpotential resulted in an increase in the band at 1608 cm^{-1} only, while other bands of the original SP remained unaffected (Figure 7.4b (v)). In addition, bands, which can be attributed to formation of the merocyanine form after oxidation, such as a strong C-O stretching band at 1197 cm^{-1}, were not observed [see Chapter 5]. The increase in the aromatic ring stretching band at 1608 cm^{-1} is consistent with the ATR FTIR spectrum of the neutral spiropyran dimers formed in solution after bulk electrolysis of **1** and was assigned to a C=C vibration of the coupled aromatic rings of the indoline moieties of the dimer **2**.

The cyclic voltammogram was paused after the first reduction wave, at 0.8 V (Figure 7.4a (iii)) to form the intermediate oxidation state of the SAM and the SERS spectrum was compared with the solution Raman spectrum of the radical cation dimer ($\mathbf{2}^{+\cdot}$). The ring vibration at 1608 cm^{-1} and a broad band at ca. 1340 cm^{-1} are similar to the Raman spectrum of radical cation dimers of TMB observed in solution [24,25] (Figure 7.4a (iii)). Notably the absolute intensity of the spectrum was much higher than the intensity of (iv) or (v), due to the excitation at 785 nm being resonant with an intense absorption of $\mathbf{2}^{+\cdot}$ in the NIR region (see UV/Vis absorption spectrum in Figure 6.2, Chapter 6). A spectrum of the SAM measured after partial oxidation at 0.8 V was identical to the spectrum (iii), supporting that reformation of the radical cation intermediate on the 2nd oxidation sweep in positive direction occurs.

The reproducibility in obtaining the neutral dimer and monocationic states was verified by generating each of these states in the SAM through five consecutive voltammetric cycles with no evidence of degradation.

UV/Vis absorption spectroelectrochemistry of a SAM on semitransparent Au/glass

UV/Vis absorption spectroscopy was carried out *in situ* to observe changes in the absorption spectrum of the SAM **3**-Au (18 nm Au/glass) upon oxidation. Initially the monolayer was formed in the neutral spiropyran form and did not absorb in the visible region (Figure 7.5a). As was shown for the oxidation of dimer **2** in solution (Figure 7.5a upper panel), the monocation and dication have distinct absorption bands in the visible range between 400-600 nm, namely a band at 516 nm for $\mathbf{2}^{2+}$ and a band centred at 478 nm for $\mathbf{2}^{+\cdot}$. Oxidation of the SAM of **3**-Au was achieved electrochemically by sweeping the potential until complete oxidation and holding at 1.0 and 0.85 V for acquisition of the spectra of the dication and monocation, respectively (Figure 7.5b). The spectrum obtained upon holding the potential at 1.0 V shows a band at 516 nm, while at 0.85 V it shows a band at 478 nm and shoulders at longer and shorter wavelength. These results are in a good agreement with spectra obtained for $\mathbf{2}^{2+}$ and $\mathbf{2}^{+\cdot}$ in solution. Sweeping towards negative potentials shows the expected reduction waves and restores the SAM to the neutral dimer form as evidenced by the absence of absorption in the visible range. Remarkably, holding the potential at 1.0 V for spectral acquisition for at least 10 min does not result in degradation, desorption or a decrease in the SAM's electrochemical response and the cycle can be repeated several times.

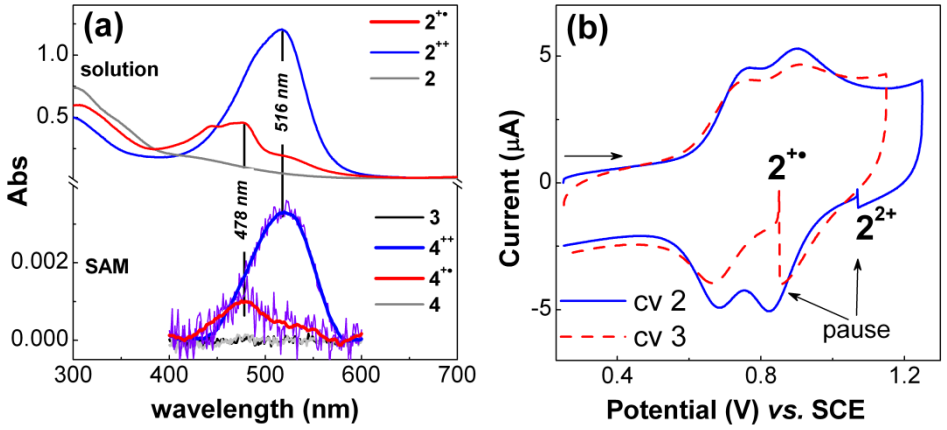

Figure 7.5 (a) Comparison of UV/Vis absorption spectroelectrochemistry of the monocation dimer $\mathbf{2}^{+\cdot}$, the dication dimer $\mathbf{2}^{++}$ and the neutral dimer of **2** obtained in acetonitrile with 0.1 M $NaClO_4$ (upper panel) and of spiropyran **3**-Au, the monocation dimer $\mathbf{4}^{+\cdot}$-Au, the dication dimer $\mathbf{4}^{++}$-Au and the neutral dimer of **4**-Au obtained in dichloromethane with 0.1 M $TBAPF_6$ (lower panel). (b) Corresponding cyclic voltammograms of **4**-Au, which were held at 1.0 and 0.85 V to obtain the dication and monocation dimer states in the SAMs, respectively.

X-ray photoelectron spectra of SAM on Au/mica

X-ray photoelectron spectroscopy on SAMs of **3** on Au/mica provided information on the composition of the SAMs, and the changes observed in the oxidation state of the indoline nitrogen of **3** through the redox cycle. XPS data obtained for the SAM of **3** after cyclic voltammetry in acetonitrile or dichloromethane with $TBAPF_6$ features contributions of solvent or tetrabutylammonium$^+$ in the N 1*s* XPS spectrum, therefore a nitrogen free solvent and supporting electrolyte – EtOH with 0.1 M $NaClO_4$ were used. The CV obtained in EtOH/$NaClO_4$ (Figure 7.6) is similar to that measured in $CH_3CN/TBAPF_6$.

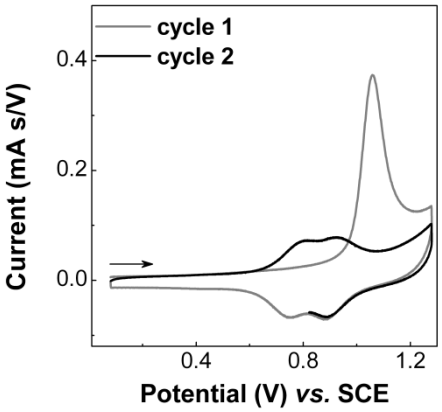

Figure 7.6 Cyclic voltammogram of SAM **3**-Au/mica measured in ethanol (0.1 M $NaClO_4$) at a scan rate 0.2 Vs^{-1}. A second cycle was used to form monocation state **4**$^{+\cdot}$-Au/mica and was stopped at 0.8 V.

In the S 2*p* region only one doublet was observed at a binding energy (BE) of 161.9 eV (4.7 at %) and assigned to the chemisorbed disulfide-Au bonding (see Figure 5.6 in Chapter 5]. In the N 1*s* core level region peaks corresponding to indolinic nitrogen and the nitrogen of nitrobenzopyran were observed at 399.4 eV and 405.9 eV BE, respectively (Figure 7.7a). The amount of nitrogen in the SAM was 5.5 at%, in agreement with the theoretical value of 5.4 at% expected based on the stoichiometry of spiropyran **3**. There was no evidence for a N^+ peak at 400.5-401 eV, which excludes the presence of the ring-open merocyanine form.

From UV/Vis absorption and SERS spectra of SAMs **3** on Au, one can conclude that upon oxidation a symmetrical dimer **4**-Au forms irreversibly, which shows reversible oxidation to the monocationic and dicationic states (Figure 7.4, Figure 7.5). To confirm the formation of the charged species and to observe where the charges are localized, **4**$^{+\cdot}$-Au and **4**$^{++}$-Au were studied by XPS.

In Figure 7.7, middle panel, a N 1*s* core level spectrum of a SAM **4**-Au, which was oxidized at 0.8 V shows that partial oxidation results in a broadening of the indoline peak at 399.4 eV. The broader peak can be fitted with two equal components at 399.0 and 399.8 eV, and assigned to the electron-rich indoline nitrogen and electron-poor indoline nitrogen respectively of the two halves of spiropyran dimer. From the binding energy of the electron-rich nitrogen (399 eV), it can be deduced that in the radical half of the dimer the

electron density is located in proximity to the nitrogen, while in the cationic half of the dimer the nitrogen has a partial positive charge. The formation of the two tautomers in the radical cation $\mathbf{2}^{+\cdot}$ is therefore occuring upon partial oxidation to the monocationic state. The first option is $\mathbf{2}^{+\cdot}\mathbf{A}$ (Scheme 7.2), in which the unpaired electron is delocalized between the two indoline moieties of the dimer due to extended conjugation. In the second, $\mathbf{2}^{+\cdot}\mathbf{B}$, the electron is localized in one moiety of the dimer with respectful positive charge on it. The observation of two separated contributions in the indoline nitrogen peak, representing the electron rich and the electron deficient indoline nitrogen atoms, favours the tautomer $\mathbf{2}^{+\cdot}\mathbf{B}$, in which the two nitrogens can be distinguished. This suggests that NIR absorption band of the radical cation (Figure 6.2, Chapter 6) may be due to optical electron transfer transitions [26]. This hypothesis seems more likely to be probable for the SAM, where dynamics of intra- and intermolecular interactions is slower than in solution.

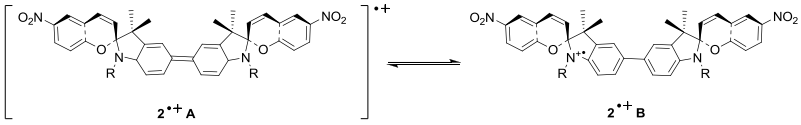

Scheme 7.2 Two representative of the radical cation of **2**: $\mathbf{2}^{+\cdot}\mathbf{A}$ with a delocalized charge distribution and $\mathbf{2}^{+\cdot}\mathbf{B}$, in which positive charge is localized on one indoline moiety.

The presence of Na^+ and ClO_4^- counterions in the SAM is evident from the Na 1*s* core level line at 1072 eV and the Cl 2*p* doublet at 208 eV in the XPS spectra shown in Figure 7.7b. The quantitative analysis of the photoemission intensities indicates that the quantities of counterions correspond stoichiometrically to $Na^+/SP = 1/(2.6\pm0.6)$ and $ClO_4^-/SP = 1/(1.8\pm0.1)$. To compensate the positive charge at the cationic moiety with ClO_4^- and a negative charge at the other part of the dimer with Na^+, a ratio of $NaClO_4/SP=1/2$ is theoretically expected. The mismatch between the expected and observed values and some fluctuation of the counterions distributions in the monolayer is attributed to the nature of the radical cation state as intermediate between neutral and dication and to the small potential window where it exists as dominant species (0.8 ±0.05 V).

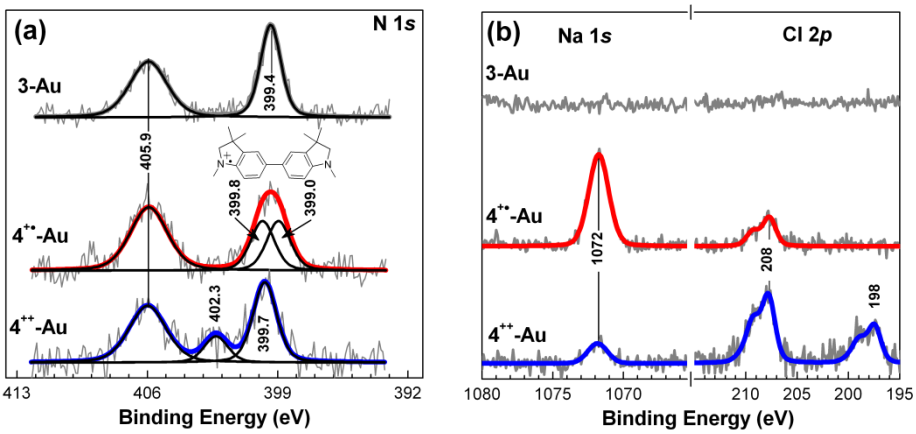

Figure 7.7 (a) XPS spectra of the N 1*s* core level region of SAM **3**-Au/mica (top panel), SAM $\mathbf{4}^{+\cdot}$-Au/mica (middle panel) and SAM $\mathbf{4}^{++}$ (bottom panel), obtained after electrochemical oxidation by pausing the potential at 0.85 V (Figure 7.6) and 1 V as in Figure 7.5b. (b) XPS spectra of N 1*s* and Cl 2*p* core level regions of SAM **3**-Au/mica (top panel), SAM $\mathbf{4}^{+\cdot}$-Au/mica (middle pannel) and SAM $\mathbf{4}^{++}$ (bottom panel).

After complete oxidation of the SAM at 1.0 V a symmetric dicationic dimer is formed. As a consequence of the absence of the neutral indoline contribution to the N 1*s* XPS spectrum (Figure 7.7a, bottom panel) the indoline nitrogen peak narrowed, and could be fit with a single component at 399.8 eV BE, which is in agreement with a partially charged N. In addition a new component at 402.3 eV is observed, indicating that 24% of the indoline nitrogen species have larger positive partial charge. The observation of a positively charged indoline nitrogen is confirmed by the presence of counterions. Complete oxidation to the dication $\mathbf{4}^{2+}$ state results in a substantial increase of the Cl 2*p* and concomitant decrease of the Na 1*s* photoemission intensities, as shown in Figure 7.7b. These changes translate into the SAM with stoichiometric ratios of SP/Cl = 1.0±0.05 and SP/Na=5.3±0.5. Notably, sweeping to higher potentials (>1 V) to obtain the dicationic dimer $\mathbf{4}^{++}$ results in the appearance of an additional component to the Cl 2*p* XPS core level region at 198 eV, corresponding to Cl in a lower oxidation state, attributed tentatively to $AuCl_2$. Therefore, the observation of positive charge on the N atoms and of a stoichiometric amount of counterions confirms the formation of the dicationic state in the SAM of the spiropyran on gold.

Reduction of the SAM to its neutral state results in a N 1*s* spectrum identical to the initial spectrum (Figure 7.7 and Figure 7.8a, top panels), as expected, because of the equivalent chemical environment of the nitrogen in the spiropyran dimer and monomer.

Photochromism of dimers in SAMs

The photochromism expected for spiropyrans was observed in solution for both monomer of spiropyran **1** and the corresponding dimer **2,** as well as for SAMs of **3** on gold by UV/Vis absorption, Raman and XPS spectroscopy [See chapters 5,6]. A SAM of **3**-Au

was oxidized electrochemically to obtain a SAM of dimer **4** and subsequently irradiated with UV light to assess whether or not if the photochromism of **3** is retained after its electrochemical dimerization in the SAM.

As shown in Figure 7.8, irradiation of a SAM **4(SP)**-Au with UV light resulted in changes in the N 1*s* region of the XPS spectrum, namely the contribution of neutral indoline nitrogen at 399.4 eV BE decreased and a new component appeared at 401.0 eV BE. Quantitative analysis indicates that the latter is present in *ca.* 31% of the molecules constituting the SAM. The new peak is in agreement with literature data for the N^+ nitrogen of the ring-open merocyanine form [see Chapter 5]. This conversion yield for the photochromic reaction in the SAM of **4** is consistent with previous results obtained with a SAM of **3** [see Chapter 5]. Irradiation with UV light results in changes to the vibrational spectrum of the SAM of spiropyran monomer **3**-Au on a roughened bead [see Figure 5.13 in Chapter 5]. The SERS spectrum recorded after electrochemical oxidation and hence dimerization to **4**-Au consists of characteristic bands of the SP dimer – a symmetric nitro stretch at 1336 cm^{-1} and a C=C-C=C indoline vibration at 1608 cm^{-1} (Figure 7.8b).* Exposure to UV light results in the appearance of features typical of the MC form, namely the C-O stretching band at 1198 cm^{-1} and the aromatic modes at *ca.* 1400-1600 cm^{-1}, and in the absence of characteristic spiropyran bands at 1336 cm^{-1}, 1227 cm^{-1} and 1650 cm^{-1}, while the persistence of the dimer aromatic band at 1608 cm^{-1} confirms the stability of the dimer under exposure to UV light.

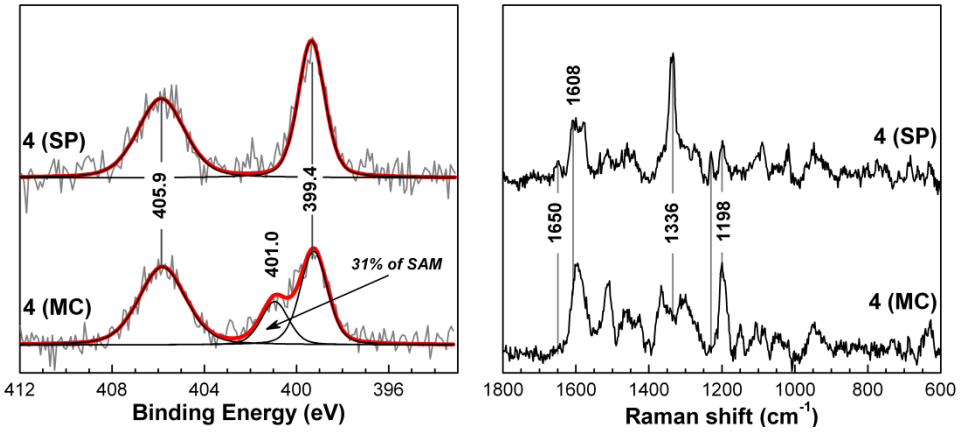

Figure 7.8 Photochromic response of dimers observed in a SAM **4**-Au/mica (a) and a SAM **4**-Au roughened bead (b). Irradiation of a SAM **4**-Au/mica at 365 nm results in the XPS spectra of the N 1*s* core level region (a) in a decrease of the indoline nitrogen component at 399.4 eV binding energy, corresponding to the SP form and a concomitant increase in the indoline nitrogen component at 401 eV, assigned to the MC form. Irradiation of a SAM of **4** on a roughened Au bead with UV light results in the SERS spectra (b) with decreased characteristic SP dimer bands and concomitant appearance of MC dimer bands.

* Note that some MC features are also observed due to unavoidable photochromic switching induced by two photon absorption of NIR light by SP analogous to that described in Chapter 5.

The observation of SP→MC photochromism in the electrochemically formed dimers in the SAM on gold holds important consequence for the applicability of spiropyrans, as the MC form can be equally effectively obtained for both the monomer or dimer form.

Electrochemistry of the MC form in a SAM on Au

Although the focus of this study has been on the electrochemistry of the spiropyran SAMs, the electrochemical behaviour of monomeric merocyanine in the SAM on Au (**3**(**MC**)-Au) was studied to explore whether the open MC structure can undergo dimerization and to identify possible products of the oxidation of a SAM after irradiation with UV light (Scheme 7.3).

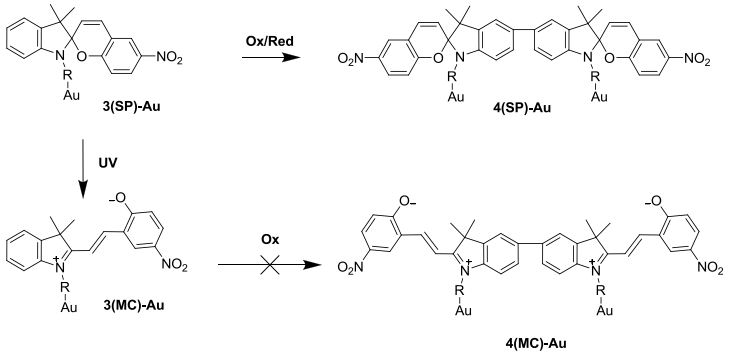

Scheme 7.3 Photochemical ring-opening of the SP form **3**(SP)-Au to the MC form **3**(MC)-Au induced by UV light and electrochemical oxidation of the obtained MC monomer.

The current density for the initial oxidation of **3**(SP)-Au was 20 ± 0.5 μA/cm^2 and the charge density related to oxidation – 8 ± 0.2 μC/cm^2. The first cycle of the cyclic voltammogram of the SAM after irradiation at 365 nm (**3**(MC)-Au in Scheme 7.3), shown in Figure 7.9, points to two differences with respect to the pristine SAM: a substantial, but incomplete (due to incomplete photochromic conversion SP→MC) decrease in the current density of the oxidation at 1.0 V and the appearance of a shoulder at 0.95 V, tentatively attributed to the oxidation of the MC form. Quantitatively, the current density decreased to 5 ± 0.2 μA/cm^2 (4 times less) with an associated charge density of 3.5 ± 0.2 μC/cm^2. Similarly the current density of the dimer redox waves at 0.75 and 0.87 V decreased. The decrease in the current density of the redox waves overall is attributed to the lower yield of dimerization in the ring-open planar MC structure. After the redox cycle it is likely that the spiropyran molecules, which were previously not subject to photochromic conversion have dimerized, as seen before, to give **4**(SP)-Au, however the product of oxidation of MC remains unclear. The proximity of the oxidation potentials of the SP and MC forms was reported previously by Zhi *et al.* [16], who did not observe differences in the electrochemistry in solution of spiropyran before and after UV irradiation.

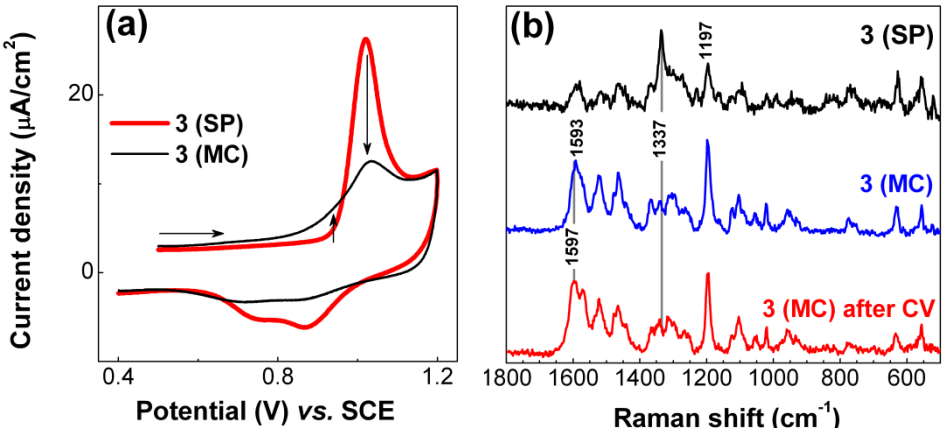

Figure 7.9 (a) Cyclic voltammogram of SAM **3**-Au/mica in spiropyran form (red line) and another pristine SAM after irradiation with UV light (black line) in dichloromethane (0.1 M $TBAPF_6$). A decrease in the spiropyran oxidation wave and increase in pre-peak at 0.95 V are indicated with arrows. (b) SERS spectrum of **3**(SP) spiropyran SAM on a roughened Au bead initially, after irradiation at 365 nm to form **3**(MC) and after oxidation cycle (**4**(MC)).

A self-assembled monolayer of spiropyran **3** on a roughened Au bead was irradiated at 365 nm to obtain the merocyanine form **3**(MC) and studied by SERS after electrochemical oxidation. As shown in Figure 7.9b, substantial changes in the vibrational spectra are observed after oxidation and reduction. Initially the monolayer is composed of the SP form, manifested in the SERS spectrum in a strong nitro stretch at 1337 cm^{-1} (top spectrum), which decreases substantially after irradiation with UV light (middle spectrum). An intense C-O stretching band at 1197 cm^{-1} and aromatic bands at 1400-1600 cm^{-1} confirm the formation of the MC form. The spectrum measured after oxidation (bottom spectrum) shows remarkably similar features to that of the MC form, but the band at 1593 cm^{-1} appears to shift to 1597 cm^{-1}. The observation that the indoline aromatic ring band shifts to higher wavenumbers in the MC form after oxidation is similar to the situation observed for the SP form, where the aromatic indoline SP band appears at higher wavenumber (1613 cm^{-1}) (see ATR FTIR spectra presented in Figure 6.4 in Chapter 6).

The cyclic voltammogram and the SERS spectrum of SAM **3**(MC) after oxidation suggest that oxidation of the MC form may result in a similar dimerization, as for the SP form. However, we can exclude that the same **4**(SP)-Au or **4**(MC)-Au conformers are formed (see Scheme 7.3) because the electrochemistry of the obtained product is not consistent with **4**(SP)-Au and thermal recovery or irradiation with visible light of the MC SAM after oxidation does not restore the redox behaviour of the spiropyran, pointing at an irreversible change in the MC form to another species upon oxidation.

Electrochemistry of MC dimers SAMs on Au

As was shown in Figure 7.3, the CV of **4**-Au features two reversible one-electron oxidations to form a dication $\mathbf{4}^{++}$ with a radical cation intermediate $\mathbf{4}^{+\cdot}$. Irradiation of the

neutral dimer results in ring-opening either only in one half of the dimer, giving rise to a species **4**(SP-MC)-Au or in both halves resulting in **4**(MC-MC)-Au) as sketched in Scheme 7.4.

The CV of a SAM **3**(SP)-Au/mica was carried out to form a SAM of **4**(SP)-Au, which was then irradiated with UV light (365 nm) to obtain dimers with the MC structure, *i.e.* **4**(SP-MC)-Au and **4**(MC-MC)-Au. The CV was then performed on the SAM obtained to observe whether it undergoes similar irreversible oxidation as the monomer SAM **3**(MC)-Au.

The cyclic voltammogram obtained after irradiation with UV light (Figure 7.10) shows substantially weaker reversible redox waves with an overall charge density of 3 ± 0.1 μC/cm^2 for the dimer peaks, which is less than half of the initial value of 7.3 ± 0.1 μC/cm^2, measured before irradiation. In comparison, the CV of the SAM of monomer **3**-Au after irradiation with UV light and oxidation shows an even lower current density of the dimer oxidation waves – 0.5 ± 0.1 μC/cm^2. This demonstrates that both sequences of the stimuli a) first irradiation and then oxidation or b) first oxidation and then irradiation give electrochemically similar results – a decrease in the oxidative response of the dimers.

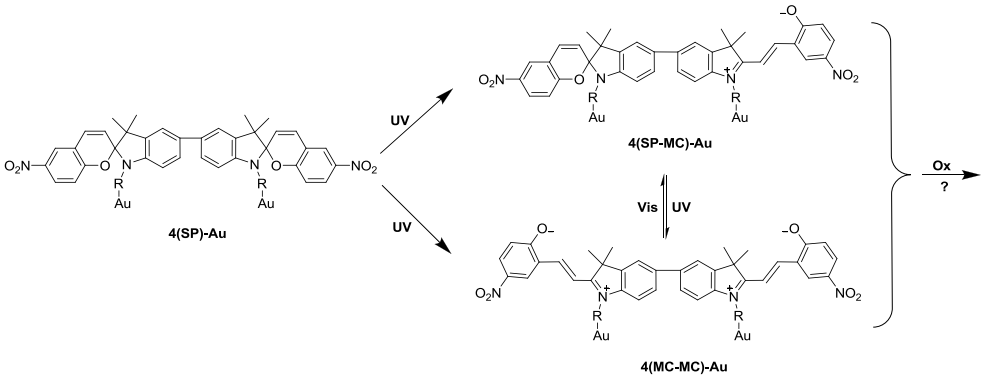

Scheme 7.4 Possible photochromic products - **4**(SP-MC)-Au and **4**(MC-MC)-Au obtained upon exposure of a dimer SAM **4**(SP)-Au to UV light.

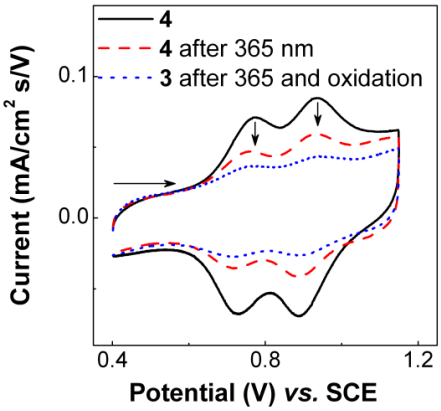

Figure 7.10 Cyclic voltammogram of dimer SAM **4**-Au/mica, formed after initial oxidation cycle on SAM **3**-Au/mica (Figure 7.9a), before (black line) and after irradiation at 365 nm (red line). A cyclic voltammogram of a SAM **3**-Au after irradiation with UV light and a subsequent oxidation cycle is shown for comparison.

7.3 Summary and outlook for utilization of the full spiropyran functionality in SAMs on Au

The most interesting result regarding the oxidation of spiropyrans in solution, namely the aryl C-C coupling to form a symmetric dimer in the ring-closed SP form and its photochromic conversion to the ring-open MC form was reproduced in the self-assembled monolayers on gold. Therefore, considering exclusively a combination of photo- and electrochemical stimuli, the following switching can be realized in the SAM **3**-Au (Scheme 7.5): (a) photochromism of monomeric SP **3**(SP)-Au↔**3**(MC)-Au [discussed in Chapter 5]; (b) irreversible oxidation of spiropyran to form double protonated symmetric dimer H_2**4**(SP)-Au, which spontaneously releases two protons resulting in **4**(SP)-Au; (c) reversible electrochemical oxidation of the dimer **4**(SP)-Au to the dicationic state $\mathbf{4}^{++}$(SP)-Au *via* a monocationic intermediate $\mathbf{4}^{+\cdot}$(SP)-Au; (d) reversible photochromism of dimer **4**(SP-SP)-Au↔**4**(SP-MC)-Au↔**4**(MC-MC)-Au; (e) irreversible oxidation of the ring-open monomeric MC form **3**(MC)-Au and (f) oxidation of the corresponding dimers of the MC form **4**(SP-MC)-Au and **4**(MC-MC)-Au.

This opens possibilities for potential applications of spiropyrans in dual responsive (monolayer) materials, molecular logic or memory. Reversible photochromism allows for temporal storage of the information, when the spiropyran is either in the monomeric or the dimeric form; irreversible oxidation leads to a new, permanent dimer state with reversible electrochemistry and photochemistry.

To complete the exploration of the full functionality of spiropyran monolayers, additional studies are on-going concerning the reduction of a SAM, the influence of the pH on the formation of the dimer and the complementary spectroscopic identification of the oxidation product of the MC form.

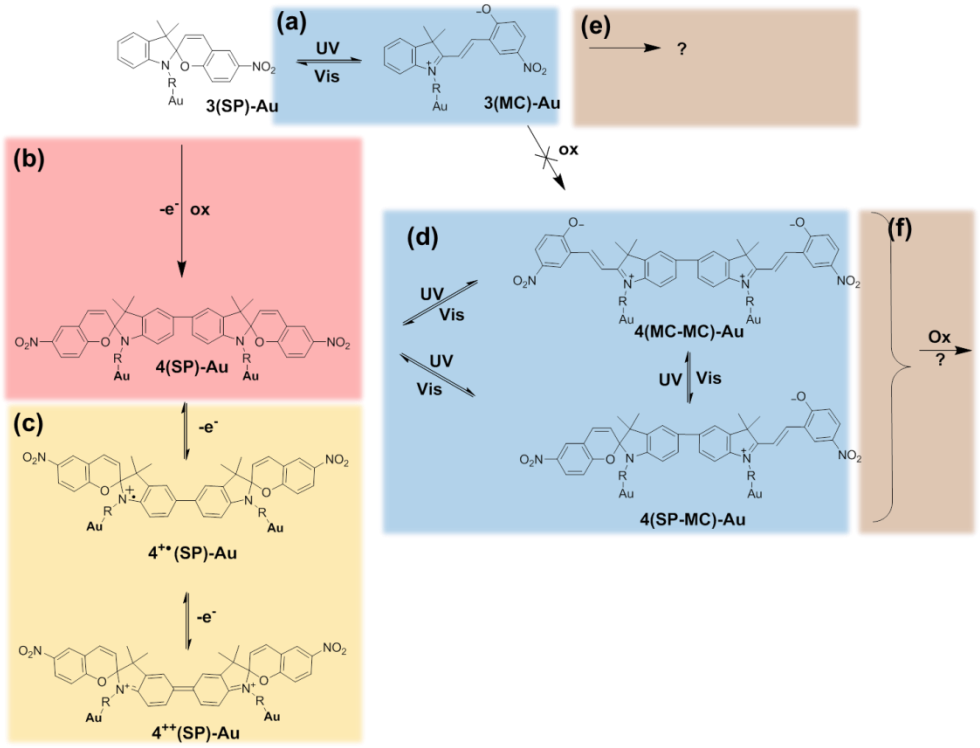

Scheme 7.5 Summary of the photoelectrochemical switching in a spiropyran SAM on gold. (a) Photochromism of monomer **3**(SP)-Au↔**3**(MC)-Au; (b) irreversible oxidation of spiropyran to form a doubly protonated symmetric dimer, H_2**4**(SP)-Au, which spontaneously releases two protons resulting in **4**(SP)-Au (see also Figure 7.1b for dimerization in solution); (c) reversible electrochemical oxidation of the dimer **4**(SP)-Au to form the dicationic state $\mathbf{4}^{++}$(SP)-Au with a monocationic intermediate $\mathbf{4}^{+\bullet}$(SP)-Au; (d) reversible photochromism of the dimer **4**(SP-SP)-Au↔**4**(SP-MC)-Au↔**4**(MC-MC)-Au; (e) Irreversible oxidation of the ring open monomeric MC form **3**(MC)-Au and (f) oxidation of the corresponding dimers of the MC form **4**(SP-MC)-Au and **4**(MC-MC)-Au.

7.4 Conclusions

Self-assembled monolayers of spiropyran were prepared on polycrystalline Au surfaces and studied spectroelectrochemically. The main question was whether oxidative dimerization of the spiropyran occurs in a SAM in the same way as in solution, or whether steric interactions and lack of surface mobility allow for the observation of a reversible electrochemistry.

The cyclic voltammetry and surface enhanced Raman scattering spectra provided direct evidence of the similarity of the oxidative dimerization in a solution and in SAMs, where irreversible oxidation of spiropyran results in a C-C coupling to form a symmetric dimer, which itself shows reversible electrochemistry. The surface coverage of $(6 \pm 1)*10^{-11}$ mol/cm^2 and an area per molecule in the SAM of 3.3 nm^2 point to a certain degree of freedom and flexibility in the SAM. At the same time, the distance between the spiropyrans allows for efficient chemical reaction between neighbouring molecules such that monomers

no longer remain on the surface after the first oxidation cycle. It may be possible to tune the reactivity of the monomer in the SAM by selecting different linkers, with which a higher surface coverage can be obtained.

In the XPS spectra a reversible change in the oxidation state of the nitrogen as well as uptake and release of counterions upon oxidation to the monocationic and dicationic states was observed. The stability of the higher oxidation states in a SAM in ultrahigh vacuum for several hours emphasizes the robustness of the SAM towards redox switching.

The direct observation of spiropyran bands in the SERS spectra of the neutral or the monocationic dimer provides support that the product of the oxidation is spiropyran in the ring-closed form and eliminates ambiguities present in the earlier literature.

Another important functionality of the spiropyran observed in solution – the photochromism of the spiropyran dimers was also reproduced in the SAM, giving rise to reversible formation of the merocyanine features in a dimer form, as manifested in both XPS and SERS spectra. This dual responsive behaviour provides an important potential for application in molecular electronics and in "smart" monolayer surfaces.

7.5 Experimental details

For comparison of the electrochemical data – current and charge densities of a pristine and irradiated SAM of **3**-Au a functionalized Au slide after monolayer formation was divided into two halves. One half was studied electrochemically as prepared, while the other was exposed to UV light prior to cyclic voltammetry. This ensured equal surface coverage for the proper comparison of CVs of pristine and irradiated SAMs.

7.6 Acknowledgements

The synthesis and NMR characterization of the monomer compounds **1** and **3** were performed by J. T. van Herpt. Details for synthetic procedures can be found in his PhD thesis or in the literature [20].

7.7 References

[1] Laviron, E.; Mugnier, Y. *J. Electroanal. Chem. Interfacial Electrochem.* **1980**, 111, 337–344.
[2] Browne, W. R.; Pollard, M. M.; de Lange, B.; Meetsma, A.; Feringa, B. L. *J. Am. Chem. Soc.* **2006**, 128, 12412–12413.
[3] Ivashenko, O.; Logtenberg, H.; Areephong, J.; Coleman, A. C.; Wesenhagen, P. V.; Geertsema, E. M.; Heureux, N.; Feringa, B. L.; Rudolf, P.; Browne, W. R. *J. Phys. Chem. C* **2011**, *115*, 22965–22975.
[4] Logtenberg, H.; Browne, W. R. *Org. Biomol. Chem.* **2013**, *11*, 233–243.
[5] Lukyanov, B. S.; Metelitsa, A. V.; Voloshin, N. A.; Alexeenko, Y. S.; Lukyanova, M. B.; Vasilyuk, G. T.; Maskevich, S. A.; Mukhanov, E. L. *Int. J. Photoenergy* **2005**, *7*, 17–22.
[6] Görner, H. *Phys. Chem. Chem. Phys.* **2001**, *3*, 416–423.
[7] Wang, D.; Jiao, P.; Wang, J.; Zhang, Q.; Feng, L.; Yang, Z. *J. Appl. Polym. Sci.* **2012**, *125*, 870–875.

[8] Byrne, R.; Ventura, C.; Benito Lopez, F.; Walther, A.; Heise, A.; Diamond, D. *Biosens. Bioelectron.* **2010**, *26*, 1392–1398.
[9] Willner, I.; Rubin, S.; Cohen, Y. *J. Am. Chem. Soc.* **1993**, *115*, 4937–4938.
[10] Darwish, T. A.; Tong, Y.; James, M.; Hanley, T. L.; Peng, Q.; Ye, S. *Langmuir* **2012**, *28*, 13852–13860.
[11] Heiligman-Rim, R.; Hirshberg, Y.; Fischer, E. *J. Phys. Chem.* **1962**, *66*, 2470–2477.
[12] Raymo, F. M.; Giordani, S. *J. Am. Chem. Soc.* **2001**, *123*, 4651–4652.
[13] Rosario, R.; Gust, D.; Hayes, M.; Springer, J.; Garcia, A. A. *Langmuir* **2003**, *19*, 8801–8806.
[14] Chibisov, A. K.; Görner, H. *Chem. Phys.* **1998**, *237*, 425–442.
[15] Doron, A.; Katz, E.; Tao, G.; Willner, I. *Langmuir* **1997**, *13*, 1783–1790.
[16] Zhi, J. F.; Baba, R.; Hashimoto, K.; Fujishima, A. *Ber. Bunsen Ges./Phys. Chem. Chem. Phys.* **1995**, *99*, 32–39.
[17] Preigh, M. J.; Stauffer, M. T.; Lin, F.-T.; Weber, S. G. *Faraday Trans.* **1996**, *92*, 3991.
[18] Wagner, K.; Byrne, R.; Zanoni, M.; Gambhir, S.; Dennany, L.; Breukers, R.; Higgins, M.; Wagner, P.; Diamond, D.; Wallace, G. G.; Officer, D. L. *J. Am. Chem. Soc.* **2011**, *133*, 5453–5462.
[19] Wang, Y.; Yu, H.; Cai, S.; Liu, Z. *Chin. Sci. Bull.* **1997**, *42*, 304–307.
[20] Ivashenko O.; van Herpt J.T.; Feringa B.L.; Rudolf P.; Browne W.R. *Langmuir*, **2013**, *in pres.*
[21] Mizoguchi, T.; Adams, R. N. *J. Am. Chem. Soc.* **1962**, *84*, 2058–2061.
[22] Galus, Z.; White, R. M.; Rowland, F. S.; Adams, R. N. *J. Am. Chem. Soc.* **1962**, *84*, 2065–2068.
[23] Yang, H.; Wipf, D. O.; Bard, A. J. *J. Electroanal. Chem.* **1992**, *331*, 913–924.
[24] Guichard, V.; Bourkba, A.; Poizat, O.; Buntinx, G. *J. Phys. Chem.* **1989**, *93*, 4429–4435.
[25] Boilet, L.; Buntinx, G.; Lapouge, C.; Lefumeux, C.; Poizat, O. *Phys. Chem. Chem. Phys.* **2003**, *5*, 834–842.
[26] Browne, W. R.; O'Boyle, N. M.; McGarvey, J. J.; Vos, J. G. *Chem. Soc. Rev.* **2005**, *34*, 641–663.